Peptides Derived from Apoptotic Bax and Bid Reproduce the Poration Activity of the Parent Full-Length Proteins

Ana J. García-Sáez,* Manuela Coraiola,† Mauro Dalla Serra,† Ismael Mingarro,* Gianfranco Menestrina,† and Jesús Salgado*

*Department of Biochemistry and Molecular Biology, University of Valencia, Burjassot, Valencia, Spain; and †ITC-CNR Institute of Biophysics, Unit at Trento, Povo, Trento, Italy

ABSTRACT Bax and Bid are proapoptotic proteins of the Bcl-2 family that regulate the release of apoptogenic factors from mitochondria. Although they localize constitutively in the cytoplasm, their apoptotic function is exerted at the mitochondrial outer membrane, and is related to their ability to form transbilayer pores. Here we report the poration activity of fragments from these two proteins, containing the first α-helix of a colicinlike hydrophobic hairpin (α-helix 5 of Bax and α-helix 6 of Bid). Both peptides readily bind to synthetic lipid vesicles, where they adopt predominantly α-helical structures and induce the release of entrapped calcein. In planar lipid membranes they form ion conducting channels, which in the case of the Bax-derived peptide are characterized by a two-stage pattern, a large conductivity and lipid-charge-dependent ionic selectivity. These features, together with the influence of intrinsic lipid curvature on the poration activity and the existence of two helical stretches of different orientations for the membrane-bound peptide, suggest that it forms mixed lipidic/peptidic pores of toroidal structure. In contrast, the assayed Bid fragment shows a markedly different behavior, characterized by the formation of discrete, steplike channels in planar lipid bilayers, as expected for a peptidic pore lined by a bundle of helices.

INTRODUCTION

Proteins of the Bcl-2 family are key regulators of apoptosis, a well-conserved physiological process responsible for programmed cell death (Adams and Cory, 1998). They exert their function by mediating the release of apoptogenic factors, like cytochrome *c*, from mitochondria, and may have opposite roles, thus being antiapoptotic (like Bcl-2, Bcl-x_L, and Bcl-w) or proapoptotic (like Bax, Bak, Bid, and Bim). All members of the Bcl-2 family share at least one of four possible homology domains (BH). Some of them localize constitutively at intracellular membranes, such as the mitochondrial outer membrane (MOM) (Bcl-2, Bcl-x_L, and Bak) and the nuclear and endoplasmic reticulum (ER) membranes (Bcl-2, Bcl-x_L), whereas others are soluble in the cytosol and translocate to the MOM in response to apoptotic stimuli (Bcl-w, Bax, Bid, and Bim) (Gross et al., 1999; Hockenbery et al., 1990; Wolter et al., 1997).

Different mechanisms of action seem to be responsible for the function of these proteins, including selective permeabilization of the MOM by means of direct pore formation or regulation of other existing pores, and induction of the mitochondrial permeability transition pore, through regulation of Ca^{2+} release from the ER stores and Ca^{2+} uptake by the mitochondria (Esposti and Dive, 2003; Oakes et al., 2003; Scorrano et al., 2003). In either case, their function appears closely related to pore formation activity. However, characterizing this activity at a molecular level is difficult due to its complexity: First, the activation of these proteins is largely connected to their ambivalent folding properties, since they are stable both in water and lipidic media, but only the structure of the inactive, water-soluble form is known so far. This structure shows some similarities with that of the pore-forming domain of colicins and the diphtheria toxin (Chou et al., 1999; McDonnell et al., 1999; Muchmore et al., 1996; Suzuki et al., 2000), which agrees with the ability of Bcl-2 proteins to form ion channels in synthetic lipid bilayers (Antonsson et al., 1997; Minn et al., 1997; Schendel et al., 1999). Second, the large structural transition from a globular, water-soluble species to a membrane-inserted species appears to be a regulated process, where different members of the Bcl-2 family interplay to give a final outcome of activation or inhibition of apoptosis (Oltvai et al., 1993). And third, the structural similarity of pro- and antiapoptotic Bcl-2 proteins and the capacity of members of the two categories to form ion channels are not easily reconcilable with their opposite functions (Lazebnik, 2001).

Among the proapoptotic proteins of the Bcl-2 family, two groups can be functionally and structurally distinguished. The group represented by Bax and Bak is involved directly in mediating the release of mitochondrial apoptogenic factors (Bouillet and Strasser, 2002a). A second group of proapoptotic proteins that contain only domain BH3, like Bid and Bim, assist the former proteins in their function by a still unresolved mechanism, for which only some general guide lines appear to be clear. BH3-only proteins are activated by posttranslational modifications in response to apoptotic stimuli (Bouillet and Strasser, 2002b). For example, under

Submitted December 30, 2004, and accepted for publication March 4, 2005.

We dedicate this article to the memory of our friend Gianfranco Menestrina, who tragically passed away in July 2004.

Address reprint requests to Jesús Salgado, Departament de Bioquímica i Biología Molecular, Facultat de Biología (Universitat de València), C/Dr. Moliner, 50 46100 Burjassot, Valencia, Spain. Tel.: 34-96-3543016; Fax: 34-96-3544635; E-mail: jesus.salgado@uv.es.

0006-3495/05/06/3976/15 $2.00

doi: 10.1529/biophysj.104.058008

normal conditions Bid exists as an inactive form in the cytosol. Proteolytic cleavage by caspase 8 releases a 15-kDa C-terminal fragment, known as tBid, that relocalizes and binds to the MOM where it is able to induce cytochrome *c* release (Gross et al., 1999). tBid, and other BH3-only proteins, may neutralize antiapoptotic Bcl-2 proteins through BH3-dependent heterodimerizations (Bouillet and Strasser, 2002b). Additionally, they may activate Bax-type proteins by direct binding via their BH3 domain. A conformational change, which involves exposure of hydrophobic groups, followed by mitochondrial targeting, insertion in the MOM, and oligomerization, is known to be necessary for the permeabilizing activity of Bax (Desagher et al., 1999). The change in conformation can occur upon interaction with lipid vesicles (Yethon et al., 2003), whereas membrane insertion, oligomerization, and pore formation need the presence of tBid and probably other, yet unknown proteins (Eskes et al., 2000).

Careful biophysical investigations have shown that Bax can promote the release of fluorescent probes and cytochrome *c* from large unilamellar lipid vesicles (LUVs) (Saito et al., 2000). This permeabilizing activity appears to be connected to the ability of Bax to multimerize. In planar phospholipid bilayers, truncated Bax (lacking its C-terminal hydrophobic tail) induces channel-like fluctuations with multiconductance states (Antonsson et al., 1997). This complex behavior is accompanied by marked decreases of voltage-dependent lifetime and linear tension of the membrane, which are largely enhanced in the case of full-length Bax (Basanez et al., 1999). Basañez et al. interpreted these results as due to Bax-induced changes in the intrinsic monolayer curvature, promoting the formation of an at least partially lipidic pore. This idea introduced a novelty about the nature of the apoptotic pore (Zimmerberg and Chernomordik, 1999), which has been subsequently supported by the dependence of the activity of Bax-type proteins on intrinsic monolayer curvature. Thus, Bax-induced membrane permeabilization is promoted by nonlamellar lipids with positive intrinsic curvature, but inhibited by lipids with negative intrinsic curvature (Basanez et al., 2002; Terrones et al., 2004). In agreement with these observations, Bax-type proteins have been found during apoptosis at outer mitochondrial scission sites (Karbowski et al., 2002), a likely location for nonbilayer lipid structures. Additionally, Bax porelike structures, claimed to be toroidal, have been recently observed by atomic force microscopy (Epand et al., 2002b).

Although in vivo tBid needs the presence of Bax-type proteins to induce release of cytochrome c, in vitro it displays, by itself, a characteristic poration activity: tBid promotes leakage of fluorescent probes from LUVs (Epand et al., 2002a) and forms ion channels in planar lipid bilayers accompanied by destabilization of the membrane (Kudla et al., 2000). Interestingly, it has been shown recently that tBid collaborates with Bax in the formation of large lipidic pores, which are enhanced by positive curvature-inducing lipids and characterized by transbilayer lipid movement (Terrones et al., 2004). Additional data also suggest that lipids play an important role in the apoptotic permeabilization of mitochondria. Thus, targeting of tBid to membranes is increased by N-myristoylation of a glycine residue and the presence of negatively charged lipids (Zha et al., 2000). Moreover, the specific mitochondrial lipid cardiolipin (CL) has been involved in the binding of tBid to the MOM (Lutter et al., 2000) and in the enhancement of membrane permeabilization in an in vitro system containing this latter protein and Bax (Kuwana et al., 2002).

Constructing coherent models of pores formed by Bcl-2 proteins is hindered by the lack of structural information about the membrane-inserted conformation of these proteins. Most accepted ideas come from their structural analogy with the bacterial toxins, which suggests that the central hairpin formed by helices $\alpha5$ and $\alpha6$ ($\alpha6$ and $\alpha7$ in the case of Bid) could be responsible for pore formation. Supporting this model, deletion of the $\alpha5$–$\alpha6$ hairpin of Bax abrogated its ability to form ion-conducting channels and to release cytochrome *c* from mitochondria (Heimlich et al., 2004). Also, the hairpin $\alpha6$–$\alpha7$ of tBid has been found to be important for mitochondrial targeting (Hu et al., 2003). In a previous study, we evaluated the capacity of different hydrophobic fragments from these proteins to insert across membranes in a model chimerical context (García-Sáez et al., 2004). When the fragments were assayed individually, transmembrane insertion was found for the first α-helix of the core hairpin, but the second, less hydrophobic one, appeared to insert in the membrane only as part of the complete hairpin (García-Sáez et al., 2004).

Here we analyze the structure and permeabilizing activity of peptides containing the fragments $\alpha5$ of Bax ($Bax^{\alpha5}$) and $\alpha6$ of Bid ($Bid^{\alpha6}$) on model lipid membranes. We find that both peptides alone are able to reproduce in part the membrane poration activity displayed by their complete parent proteins. The characteristics of the channels induced by $Bax^{\alpha5}$ indicate that this peptide forms toroidal lipidic pores similar to the ones suggested for full-length Bax and other Bax-type proteins. In contrast, the channels formed by $Bid^{\alpha6}$ follow a different mechanism, probably by organizing into a bundle of helices.

MATERIALS AND METHODS

Peptide synthesis and purification

The peptides corresponding to fragments $Bax^{\alpha5}$ (sequence Ac-KGR-VVALFYFASKLVLKALSTKVPELIRTK-NH_2) and $Bid^{\alpha6}$ (sequence Ac-EKEKTMLVLALLLAKKVASHYPS-NH_2) were prepared by automatic solid-phase synthesis according to previously reported protocols (Orzaez et al., 2004). $Bax^{\alpha5}$ consisted of residues Gly^{108}–Thr^{135} from the sequence of human Bax (numbering from the full-length protein), where Cys^{126} was changed to Ser to avoid disulfide formation. Additionally, one lysine was added on each side to improve water solubility and facilitate peptide

purification and handling (Melnyk et al., 2001; Orzaez et al., 2004). The Bid$^{\alpha 6}$ fragment contained residues Glu^{143}–Ser^{165} from human Bid (numbering from the full-length protein), with Thr^{163} changed to Tyr to allow the spectroscopic determination of the concentration of the peptide (see below).

Unless otherwise indicated, all reagents and solvents used for the peptide synthesis were from Applied Biosystems (Foster City, CA). Solid-phase synthesis of the peptides was performed on an Applied Biosystems 433A peptide synthesizer using Fmoc chemistry and Tentagel S-RAM (Rapp Polymere, Tübingen, Germany) resin (0.24 meq/g substitution) as a solid support. A sixfold molar excess of amino acids (Senn Chemicals, Dielsdorf, Switzerland) was used, and double and triple couplings were applied for difficult residues (Fisher and Engelman, 2001). Both the Bax$^{\alpha 5}$ and Bid$^{\alpha 6}$ peptides were N-terminal acetylated and C-terminal amidated. Deprotection and cleavage reactions were carried out in a mixture of 70% trifluoroacetic acid, 20% dichloromethane, 5% water, 2.5% triisobutylsilane, and 2.5% ethanedithiol (v/v), all from Merck (Whitehouse Station, NJ). Cleaved peptides were precipitated in ice-cold t-butyl-methyl ether and centrifuged. Pellets were dried, redissolved in water:acetonitrile (90:10), and lyophilized. Peptides were purified using a C18 preparative reverse-phase high-performance liquid chromatography (RP-HPLC) column to a purity of ~95% as determined by analytical RP-HPLC. Purified peptides were analyzed by mass spectrometry to confirm their molecular mass.

All peptide concentrations were determined from ultraviolet spectra using a Jasco spectrophotometer and a molar extinction coefficient $\varepsilon_{276nm} = 1450\ M^{-1}\ cm^{-1}$ for both Bax$^{\alpha 5}$ and Bid$^{\alpha 6}$.

Preparation and size measurement of lipid vesicles

All lipids used were from Avanti Polar Lipids (Alabaster, AL), except for asolectin, which was purchased from Sigma-Aldrich (St. Louis, MO) and further purified according to Kagawa and Racker (1971). LUVs were prepared as described previously (Dalla Serra and Menestrina, 2003). Briefly, lipids were dissolved in chloroform, mixed to the desired molar composition, and vacuum-dried to a film on the bottom of a round glass flask. Further drying was accomplished under strong vacuum (30 min). Lipids were resuspended to a concentration of 4 mg/mL in a solution containing 80 mM calcein, neutralized with NaOH. After six cycles of freezing and thawing, they were passed 31 times through two stacked polycarbonate filters of 100-nm pore size, using a two-syringe extruder from Avestin (Ottawa, Canada). To remove external nonencapsulated dye, LUVs were washed in Sephadex-G50 (Sigma-Aldrich) minicolumns, previously equilibrated in 140 mM NaCl, 20 mM Hepes, 1 mM EDTA, pH 7 (buffer A). The size of vesicles was measured by quasielastic light scattering at a fixed angle (90°) and at room temperature, using a laser particle sizer (Malvern Z-sizer 3, Malvern, UK) upgraded with a 30-mW laser diode emitting at 675 nm. Data analysis allowed estimation of the hydrodynamic radius from the diffusion coefficient of the particles, using the method of cumulants (Santos and Castanho, 1996) and the Stokes-Einstein equation.

Permeabilization of unilamellar lipid vesicles

The permeabilizing activity of the peptides was assayed by measuring the release of calcein from LUVs. A 96-well microtiter plate was filled with 100 μL of buffer A containing the desired amount of peptide. To avoid nonspecific interactions of the peptides and vesicles with the plastic walls, microplates were pretreated with a 0.1 mg/mL Prionex (Pentapharm, Basel, Switzerland) solution for 30 min. All experiments were done at room temperature. After adding 100 μL of LUVs, at a final lipid concentration between 2 and 5 μg/mL, the time course of calcein release was measured as the increase in fluorescence emission at 520 nm with the excitation set at 495 nm, using a fluorescence microplate reader (Fluostar; BMG, Munich, Germany). The percentage of peptide-induced calcein release ($\%R$) was calculated by:

$$\%R = 100(F_f - F_i)/(F_m - F_i), \quad (1)$$

where F_f is the value of fluorescence measured after 1 h of incubation of vesicles in the presence of the desired amount of peptides, F_i is the background fluorescence in the absence of the peptides, and F_m is the maximal fluorescence obtained in the presence of 1 mM Triton X-100. The spontaneous release of calcein was negligible in all cases.

Electrical recordings of ion channel activity

Electrical properties of Bax$^{\alpha 5}$ and Bid$^{\alpha 6}$ were measured on planar lipid membranes as reported by Dalla Serra and Menestrina (2000). Experiments were done at room temperature with solvent-free bilayers composed of asolectin, or 1,2 diphytanoyl-*sn*-glycerophosphocholine (DPhPC), or DPhPC/phosphatidic acid (PA) in a 4:1 molar ratio. Membranes were bathed symmetrically by 2 mL of buffer A. Peptides were added always on the *cys* side to stable preformed membranes with typical capacitance of 100 pF. Macroscopic currents were measured with a patch-clamp amplifier (Axon Instruments, Union City, CA). The current traces were filtered at 100 Hz and directly acquired by a computer using Axoscope 8 software (Axon Instruments). Same traces were also acquired at higher frequency and stored on a magnetic DAT tape to allow reanalysis of the fast events, eventually present. For determination of ionic selectivity, reverse voltages were measured in an increasing NaCl gradient (with the higher salt concentration in the *trans* side) and translated into a permeability ratio, P+/P− (where P+ and P− refer to cation and anion permeability, respectively), by the Goldmann-Hodgkin-Katz equation (Dalla Serra and Menestrina, 2000).

Circular dichroism spectroscopy

Samples for circular dichroism (CD) spectroscopy were prepared at a 30 μM concentration of peptide in 10 mM phosphate buffer at pH 7. Several percentages of trifluoroethanol (TFE), or different concentrations of sodium dodecylsulfate (SDS), under and above the critical micellar concentration, were added to the corresponding samples. Spectra were measured at 20°C on a Jasco J-810 CD spectropolarimeter, using a 1-mm pathlength cell. Data were collected every 0.2 nm at 100 nm/min from 250 to 185 nm, with a band width of 1 nm, and results were averaged from 10 scans. Data analysis was performed with the help of the CDPro software package, which contains three commonly used programs: SELCON3, CONTIN/LL, and CDSSTR (Sreerama and Woody, 2000, 2004). This software allows the use of different reference sets of proteins, including membrane proteins, to increase the reliability of the analysis.

Fourier-transform infrared spectroscopy experiments

Fourier-transform infrared (FTIR) spectroscopy was used to assess the secondary structure of peptides either in the lipid-mimetic solvent TFE or in aqueous buffer, or adsorbed to the lipid phase. This was done by analysis of the amide I′ band as described previously (Menestrina et al., 1999). LUVs composed of either egg phosphatidylcholine (PC) or mixtures of PC and phosphatidic acid (PA) in a 1:1 molar ratio were prepared following the procedure described above, except that the lipids were resuspended in buffer A. Each peptide was incubated for 1 h at room temperature with LUVs, at a 1:50 mol/mol protein/lipid ratio, in buffer A. The mixtures were centrifuged in an Optima TL ultracentrifuge (Beckman Instruments, Fullerton, CA), using a fixed-angle rotor (TLA-100.2), at 350 000 *g* for 3 h at 4°C. After centrifugation, the pellet was resuspended in 100 μl of 10 mM HEPES, pH 7.0 (buffer B). Samples were deposited on 10-reflection germanium crystals (45° cut) and gently dried by nitrogen flushing. For the samples in aqueous environment, the same quantity of peptide was dissolved in buffer A and directly deposited onto the germanium crystal. The latter

samples were also used to measure the spectra in lipid-mimetic environments, by redissolving them with TFE directly on the crystal surface followed by drying. Spectra of hydrated and deuterated films were collected, in an attenuated total reflection (ATR) geometry, using an FTS 185 spectrometer (Bio-Rad, Hercules, CA), with MCT-detector.

For the polarization experiments, a rotating KRS5 wire-grid polarizer was interposed and set either at 0° or 90° (with respect to the plane of internal reflections). The orientation of a structural element was calculated only for lipid-bound peptides. It was estimated from the dichroic ratio $R = A_{0°}/A_{90°}$, where $A_{0°}$ and $A_{90°}$ are the absorptions pertaining to the functional group of that element, in the parallel and perpendicular configurations, respectively (Goormaghtigh et al., 1999; Tamm and Tatulian, 1997). From R, we derived the form factor, S, which was then used to calculate the average tilt angle, γ, as in Axelsen et al. (1995).

To estimate the secondary structure content, the amide I′ band in the region 1700–1600 cm^{-1} was deconvoluted into a set of Lorentzian components, whose frequencies were assigned to different structural elements in the standard way (Menestrina et al., 1999). In particular, we used the following assignments: band at 1680 ± 3 cm^{-1}, β-turn; bands in the region 1656–1646 cm^{-1}, α-helix; band at 1640 ± 5 cm^{-1}, random coil; band at ~1610 ± 5 cm^{-1}, side-chain contribution. In addition, we observed two bands, a major one at ~1624 cm^{-1} and a minor one at 1692 cm^{-1}, which are typical of aggregated peptides in an extended conformation and correspond to strong interstrand and intrastrand interactions (Gordon et al., 2002; Tamm and Tatulian, 1997). This set of Lorentzians was used to best fit the original spectrum and the resulting relative areas were taken as the proportion of the related structure present. The small side-chain band was excluded from the normalization. In some cases, a single band at 1672 cm^{-1} was observed, indicating the presence of some trifluoroacetic acid remaining from the synthesis (Goormaghtigh et al., 1999). Such a minor band was digitally removed before analysis.

A curve fit was used to calculate the percentage of peptide aggregation. The aggregated peptide is represented by the bands at ~1624 and 1692 cm^{-1}, and the nonaggregated one by all the remaining amide I′ components in the region extending from 1630 to 1690 cm^{-1}. Due to the centrifugation procedure used for sample preparation, in the peptide-lipid samples the nonaggregated part represents lipid-bound peptide only, whereas the aggregated part may correspond to both lipid-attached aggregates and other aggregates already present in the aqueous phase that might coprecipitate.

For the peptide-lipid samples, the spectrum of the peptide was obtained after subtracting the contribution of the lipids alone, with a weight that minimizes the band remaining at 1738 cm^{-1} (stretching of the carbonyl groups in phospholipids). This was necessary in view of the high lipid/peptide (L/P) ratio. On the other hand, and for the same reason, it was not necessary to substract the peptide spectrum from the lipid-peptide one, to calculate the lipid contribution in the methylene C-H stretching region (from 3000 to 2800 cm^{-1}). The L/P ratio in the pellet was calculated by the following algorithm (Rodionova et al., 1995; Tamm and Tatulian, 1993):

$$L/P = 0.208(n_{res} - 1)\frac{(1 - S_{amide\ I'})}{(1 + S_L/2)}\frac{\int_{2800}^{2980} A_{90°}(\nu_L)d\nu}{\int_{1600}^{1690} A_{90°}(\nu_{amide\ I'})d\nu}, \quad (2)$$

where n_{res} is the number of residues of the peptide (i.e., 23 and 30 for $Bid^{\alpha 6}$ and $Bax^{\alpha 5}$, respectively), $A_{90°}$ is the absorption with the 90° polarization, and S_L and $S_{amide\ I'}$ are order parameters calculated from the ratio of the parallel and perpendicular absorption bands. S_L corresponds to the lipid chains, and is derived either from the symmetric and asymmetric CH_2 stretching (bands centered at 2853 and 2923 cm^{-1}) or from the symmetric CH_3 stretching at 2872 cm^{-1}, using θ (the angle between the direction of the dipole moment change and that of the long axis of the molecule) set at 90° or 0°, respectively. $S_{amide\ I'}$ is the order parameter for the amide I′ band (with $\theta = 0°$). The integral with suffix L was calculated from the spectrum of the lipid alone, and that with suffix amide I′ from the spectrum of the nonaggregated peptide alone (i.e., after subtracting the lipid and the aggregated peptide). The order parameter for the α-helix, S_α, was obtained using the corresponding Lorentzian components with $\theta = 30°$ (Axelsen et al., 1995; Frey and Tamm, 1991; Menikh et al., 1997).

RESULTS

Helices α5 of Bax and α6 of Bid induce permeabilization of lipid vesicles

Helices α5 from Bax and α6 from Bid form the N-terminal half of the double-helix hairpins that are considered to be the pore-forming domains of these two proteins. They are predominantly hydrophobic and have been shown to be able to act as transmembrane fragments in model chimeric systems (García-Sáez et al., 2004). To study their interaction with synthetic lipid vesicles, we synthesized two peptides ($Bax^{\alpha 5}$ and $Bid^{\alpha 6}$) that include the sequences of these fragments (see Materials and Methods).

Permeabilization of model membranes at a macroscopic level was studied by measuring the release of calcein from LUVs of different lipid compositions. In all cases, $Bax^{\alpha 5}$ and $Bid^{\alpha 6}$ induced efflux of the fluorescent dye, although the Bax peptide displayed higher poration activity (Fig. 1). Thus, $Bax^{\alpha 5}$ provoked calcein outflow at nanomolar concentrations, whereas the activity of $Bid^{\alpha 6}$ is observed at concentrations two orders of magnitude higher. Additionally, the activities of the two peptides displayed markedly different responses to changes of lipid properties. To better understand the influence of the lipidic environment, the effect of the lipid composition of the LUVs was systematically analyzed.

Influence of lipid charge

Because both $Bax^{\alpha 5}$ and $Bid^{\alpha 6}$ present a net positive charge at neutral pH, an effect of net lipid charge on the activity of these peptides was expected. Thus, release of calcein was measured for LUVs made of pure PC (neutral), mixtures of

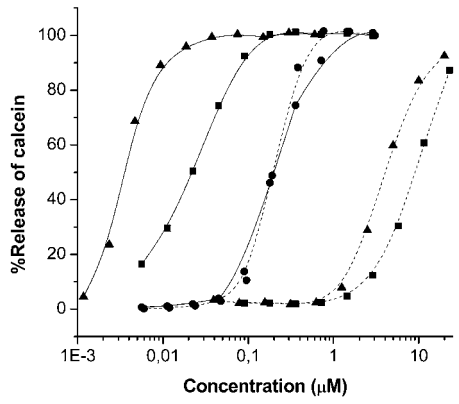

FIGURE 1 Effects of lipidic composition on the permeability of LUVs exerted by $Bax^{\alpha 5}$ (*solid lines*) and $Bid^{\alpha 6}$ (*dashed lines*). The percentage of calcein release, according to Eq. 1, is represented as a function of the concentration of added peptide. Vesicles were prepared with the following compositions: (■) PC, (●) PA, and (▲) PC/LPC (80:20).

PC and the negatively charged PA, phosphatidylserine (PS), and CL, and pure PA. The expected effect of lipid charge was found in the case of $Bid^{\alpha 6}$, which exhibited an enhanced calcein release in vesicles containing negatively charged lipids with respect to the neutral liposomes (see Table 1). This indicates a significant influence of electrostatic forces in the activity of this peptide. In contrast, the poration activity of $Bax^{\alpha 5}$ was reduced by the negatively charged lipids (Table 1). This latter effect is small in the case of PS, and significantly larger in the cases of PA and CL.

Effect of intrinsic monolayer curvature

The poration activity of full-length Bax and Bax-type proteins is greatly influenced by the intrinsic monolayer curvature of membrane lipids. Concretely, the presence of lipids with a positive intrinsic curvature, like lysophospholipids, enhances Bax activity, whereas the opposite is observed for lipids with a negative intrinsic curvature (Basanez et al., 1999). To investigate the role of intrinsic lipid curvature in the pores induced by $Bax^{\alpha 5}$, we carried out experiments of release of calcein from PC LUVs containing increasing concentrations of lysophosphocholine (LPC), positively curved, or phosphatidylethanolamine (PE), negatively curved. As shown in Fig. 1, a large increase (near sixfold) of the permeabilizing activity of the $Bax^{\alpha 5}$ peptide was observed in the presence of LPC. This marked effect was seen already at a 5% molar ratio of the lysophospholipid, with a much smaller increase between this ratio and 20% (Table 1). However, in the presence of PE, up to a 50% molar ratio, a small increase of activity was found, and the only sign of reduction of activity associated with this lipid was found in ternary lipid mixtures of PC/LPC/PE (40:40:20), where the enhancing effect induced by LPC appears to be attenuated by the presence of PE (Table 1). In contrast, when the LPC and PE-containing vesicles were assayed for the activity of $Bid^{\alpha 6}$, only small increments of the calcein release were observed (Fig. 1 and Table 1). These results show that spontaneous lipid curvature affects mainly the permeabilizing activity of $Bax^{\alpha 5}$, being principally enhanced by positive intrinsic curvature.

TABLE 1 Permeabilization activity of $Bax^{\alpha 5}$ and $Bid^{\alpha 6}$ on LUVs of different composition

Lipidic composition*	Activity, $1/C_{50}$ (μM^{-1})†	
	$Bid^{\alpha 6}$	$Bax^{\alpha 5}$
Effect of lipid net charge		
PC	0.19	46.5
PC/PS (75:25)	2.85	43.0
PC/PS (50:50)	6.07	28.0
PC/PS (25:75)	7.69	21.3
PA	5.05	5.2
PC/PA (50:50)	1.93	13.3
PC/CL (90:10)	0.80	10.9
Effect of intrinsic monolayer curvature		
PC/lysoPC (95:5)	0.11	185.2
PC/lysoPC (90:10)	0.18	238.1
PC/lysoPC (80:20)	0.25	285.7
PC/PE (95:5)	0.24	52.1
PC/PE (75:25)	0.25	56.4
PC/PE (50:50)	0.48	63.5
PC/PE/lysoPC (40:40:20)	0.64	158.7
Others		
DPhPC	0.05	0.42
Asolectin	2.05	28.6

*Lipid mixtures are reported on a molar basis.
†C_{50} is defined as the micromolar concentration of the particular peptide causing 50% of calcein release. Typical standard deviations of the reported $1/C_{50}$ values were 8–12%.

Ion channel activity of $Bax^{\alpha 5}$ and $Bid^{\alpha 6}$ in planar lipid bilayers

To study the behavior of both peptides at a microscopic level, we performed experiments using planar lipid bilayers. This technique allows the characterization of single-channel properties, such as voltage dependence and ionic selectivity (Dalla Serra and Menestrina, 2003).

With planar bilayers made of DPhPC, which easily forms stable membranes, the number of channel events induced by $Bax^{\alpha 5}$ was very low, and negligible in the case of $Bid^{\alpha 6}$ (not shown). In agreement with this behavior, both peptides displayed a reduced release of calcein from LUVs containing DPhPC, compared to LUVs made of PC alone (Table 1). However, when bilayers made of PC/PA (4:1 molar ratio) or asolectin (a natural mixture of plant lipids) were assayed, the two peptides exhibited channel activity. We had previously tested asolectin membranes for calcein release from LUVs (Table 1).

Just upon addition of $Bax^{\alpha 5}$ to asolectin planar bilayers, it demonstrated interaction with the membranes at low positive potentials. Yet, from +10 mV on, a continuous increase in the current was observed. This behavior was maintained at higher voltages and the slope current/time increased also with the potential applied. However, such an effect was absent at negative potentials, for which no currents were seen, whereas the same level of currents was recovered when we changed again to positive voltages (Fig. 2 *A*). These results suggest that positive voltages induce adsorption of $Bax^{\alpha 5}$ to the lipid bilayer and formation of microchannels. In this state, the peptide remains attached to the membrane at negative potentials, although no discrete channel activity occurs at these latter conditions. The current/voltage plot of such a conductance state revealed some voltage dependence, as shown in Fig. 2 *C*.

At a certain point, probably when the concentration of $Bax^{\alpha 5}$ attached to the membrane achieved a critical level, very high conductance pores were observed (Fig. 2 *B*), which varied between 0.3 and 5 nS. The current/voltage characteristics obtained for this second state are given in Fig. 2 *C*, which shows no voltage dependence of the single-channel

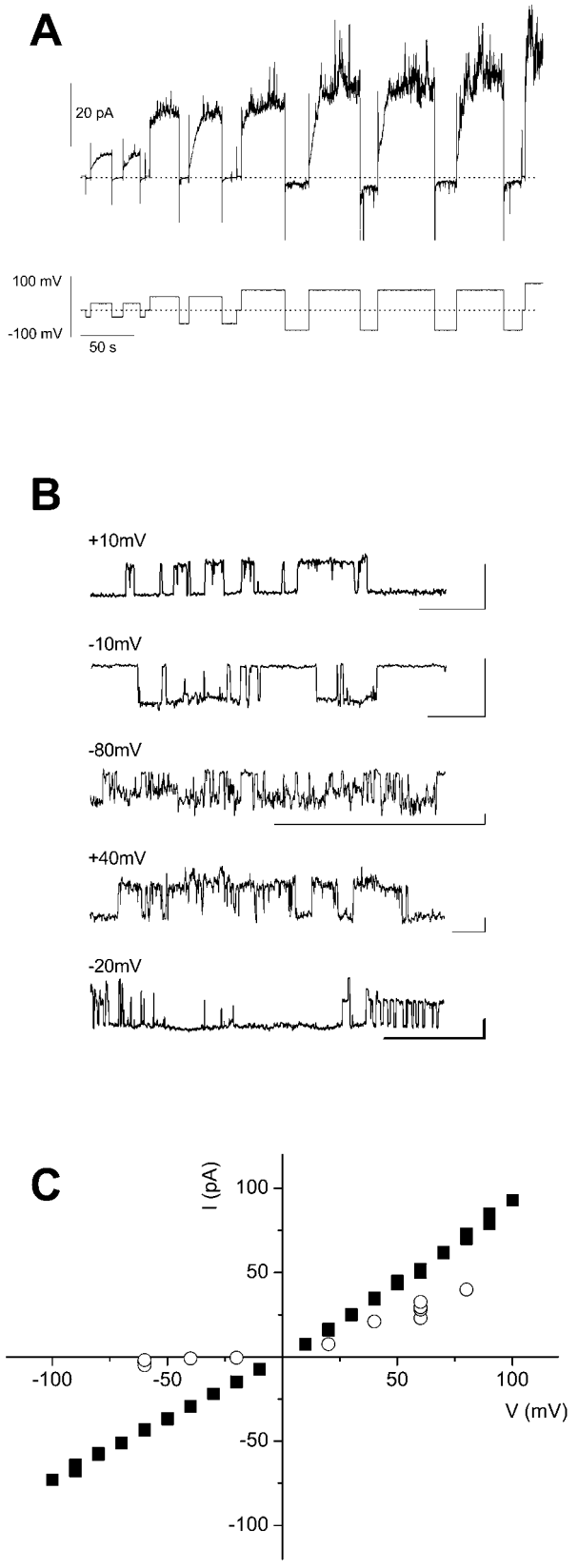

FIGURE 2 Formation of ion channels by Bax$^{\alpha 5}$ in planar lipid membranes. Addition of Bax$^{\alpha 5}$ to the buffer bathing the *cis* side of asolectin planar lipid membranes increases the ion flux across the bilayer. (*A*) Just upon addition of the peptide, a microchannel-like increase in the ion current was observed at positive potentials. (*B*) Step-like current increases corresponding to the opening of one large single channel (0.3–5 nS) were observed at several voltages, as indicated in the traces. The reference scales on the bottom right of the traces indicate 5 pA on the *y* axis and 2 s on the *x* axis, except in the last trace, where the thicker scale refers to 50 pA on the *y* axis and 20 s on the *x* axis. (*C*) Current/voltage representation of the different permeabilizing activities corresponding to *A* (○) and *B* (■).

TABLE 2 Ion selectivity of Bax$^{\alpha 5}$ in planar lipid membranes

	P+/P−[†]	
[NaCl] (M)*	Asolectin[‡]	DPhPC[‡]
0.27	6.5	–
0.43	5.9	1.0
0.57	6.2	1.0
0.70	6.2	1.1
0.82	6.3	1.4
0.93	–	1.8

*Saline concentration on the *trans* side. On the *cis* side, [NaCl] was always 0.140 M.
[†]Ratio between the permeability to cations (P+) and permeability to anions (P−) that expresses the ionic selectivity. Values >1 indicate a cation-selective channel. Values <1 indicate that the channel is selective for anions. A ratio of 1 indicates no selectivity for cations or anions.
[‡]Membrane composition.

conductance. This channel stayed open for a long time at both positive and negative voltages, revealing a different behavior from the fluctuations seen before, and eventually provoked membrane disruption.

The permeabilizing effect of Bax$^{\alpha 5}$ on planar lipid membranes was unexpected for typical ion channels, which usually show more discrete and reproducible conductance states and do not affect membrane stability, at least at low concentrations. A likely possibility is that toroidal pores are being formed, in which both the peptide and membrane lipids are involved (Basanez et al., 1999). If this is indeed the case, the ionic selectivity of the pores should depend on the electrical charge of the membrane lipids. To test this hypothesis, we measured the ionic selectivity in neutral and negatively charged membranes (Anderluh et al., 2003). We found that pores were cation-selective in asolectin membranes (negatively charged), but showed no selectivity on DPhPC membranes (neutral) (see Table 2). This effect strongly suggests that the pore lumen is lined by both peptide molecules and lipid headgroups.

In the case of Bid$^{\alpha 6}$, different channel characteristics were again observed as compared to Bax$^{\alpha 5}$. Addition of the peptide to the solution bathing a PC/PA (4:1 molar ratio) planar bilayer produced the opening and closure of different discrete channels of small conductance. Up to eight step currentlike transitions, representative of ion channel formation, were observed to be simultaneously open (Fig. 3). The statistical analysis of these transitions led to an estimation of the conductivity comprised between 13 and 15 pS. These

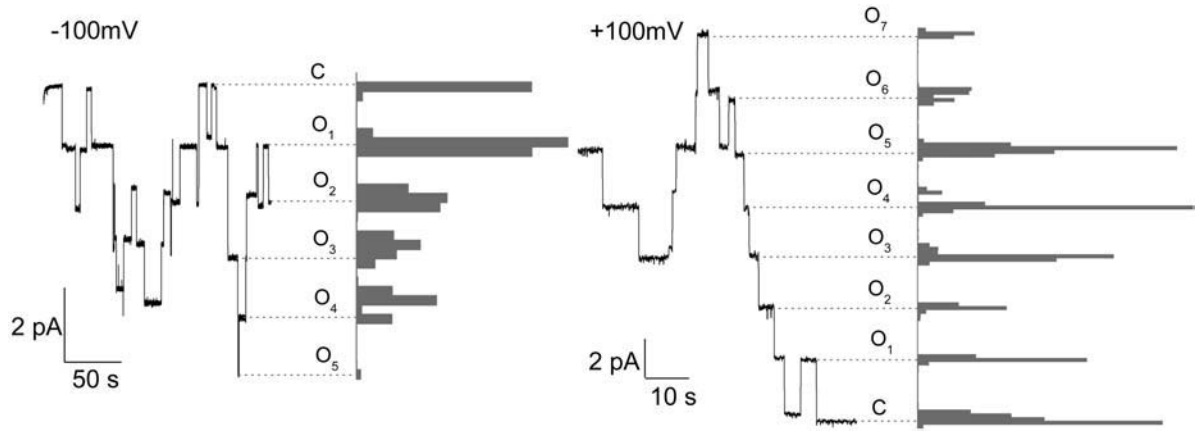

FIGURE 3 Ion channel activity displayed by Bid$^{\alpha6}$ in planar lipid membranes. When a solution containing Bid$^{\alpha6}$ was added to the buffer bathing the *cis* side of the membrane, discrete increases of the ionic current through the bilayer were observed. Each step-like current increase corresponded to the opening of one single channel with an average conductance of 13–15 pS. The closed state (*C*) and the different open levels (O_i) are marked with dotted lines, where *i* is the number of single channels simultaneously open at the indicated voltages. On the righthand side, the occupation histogram of each level is reported. The membrane composition was PC/PA (1:1).

channels opened equally at both positive and negative potentials in a voltage-independent channel-gating manner.

Structural characterization

CD spectra

The secondary structure of Bax$^{\alpha5}$ and Bid$^{\alpha6}$ was analyzed by CD in aqueous media (Fig. 4, *dotted lines*) and in the presence of different concentrations of TFE (Fig. 4, *A* and *C*) or SDS (Fig. 4, *B* and *D*). Both lipid-mimetic environments induce a large change in the conformation of the peptides with respect to the spectra in water, which is globally consistent with an increase of the α-helical structure.

To obtain a more detailed structural description, the CD spectra were analyzed by using the CDPro suite of programs (SELCON3, CONTIN/LL, and CDSSTR) (Sreerama and Woody, 2000, 2004). Similar results were obtained with the three programs and using two different reference sets of proteins: SMP50, which includes 37 soluble and 13 membrane proteins, and SDP42, a set of 42 soluble proteins, which supports the reliability of the structure estimation. Finally, the results obtained from the use of the different methods were averaged for each peptide.

In aqueous media, Bax$^{\alpha5}$ contains ~5% helical structure, being predominantly in a disordered state. However, the presence of TFE (up to 60%, Fig. 4 *A*) induces over 60% helical conformation, of which ~20% corresponds to a distorted α-helix. A similar effect was observed for samples containing up to 8 mM SDS (Fig. 4 *B*), where >50% of the peptide conformation was α-helical, even below the critical micellar concentration. In the case of Bid$^{\alpha6}$, ~50% of the peptide presents a random-coil structure in aqueous buffer, whereas the helical fraction reaches ~20%. The addition of TFE again induces an increase of the helical content, which reaches values >80%, with ~25% corresponding to a distorted α-helix (Fig. 4 *C*). In SDS (Fig. 4 *D*), high levels of helical structure also appear, amounting to ~75%.

FTIR spectra

FTIR spectra were obtained for Bid$^{\alpha6}$ and Bax$^{\alpha5}$, either in aqueous buffer or in TFE solvent (Fig. 5). For the two peptides, structural changes were evident when comparing the spectra in both media. The secondary structure composition was estimated by deconvolution and curve-fitting with a set of single Lorentzian components, which were then attributed to different structural elements (Fig. 5 and Table 3). In the case of Bid$^{\alpha6}$, we observed the presence of a large aggregated β-sheet component that was resistant to TFE and amounted to ~40% of the peptide. Passing from the aqueous buffer to TFE, the nonaggregated portion showed a strong increase in the α-helix content, from 30% to >70%, and a corresponding decrease of the random coil component. In the case of Bax$^{\alpha5}$, on the other hand, the main difference was a significant decrease of the β-sheet aggregates in TFE as compared to the aqueous buffer (from 40% to 20%), whereas the distribution of secondary structures in the nonaggregated part remained almost the same, i.e., 13% β-turn, 60% α-helix, and 27% random coil. Interestingly, in Bax$^{\alpha5}$ the α-helical structure was represented by two bands, one at ~1656 cm^{-1} (α_1) and the other at 1646 cm^{-1} (α_2). Although the former, like that of Bid$^{\alpha6}$, was in a range typical for α-helix, the latter had an unusually low frequency, which, however, has been observed already in other membrane-binding peptides, e.g., melittin (Sharon et al., 1999).

Peptides cosedimented with LUVs of PC or PC/PA (1:1) were next analyzed. A significant association of Bid$^{\alpha6}$ to PC/PA LUVs was observed. The lipid/peptide molar ratio in the pellet, estimated using Eq. 2, was ~55, very similar to the

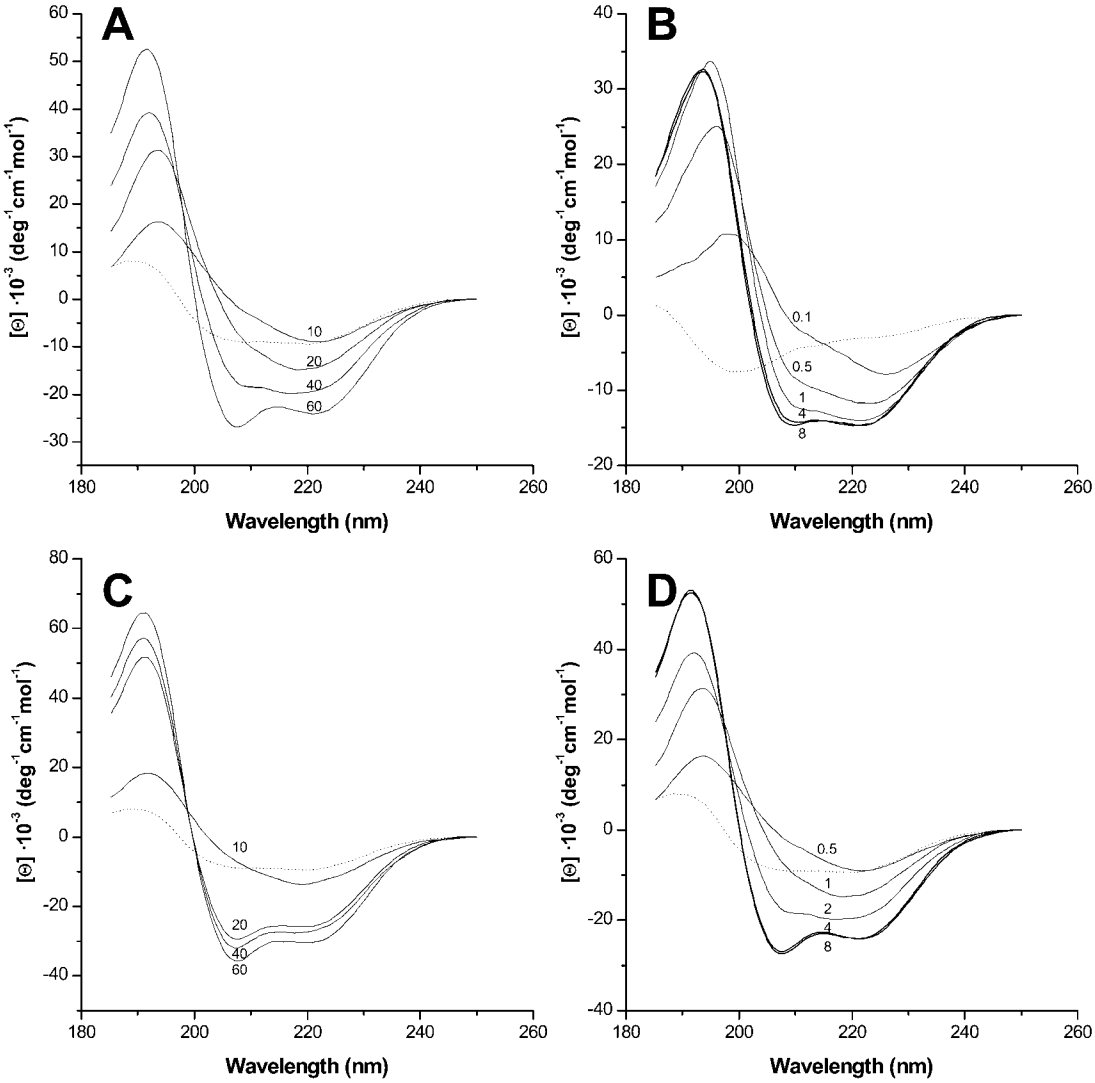

FIGURE 4 CD spectra of Bax$^{\alpha5}$ and Bid$^{\alpha6}$ in lipid-mimetic media. *A* and *C* show spectra of Bax$^{\alpha5}$ and Bid$^{\alpha6}$, respectively, recorded in aqueous buffer in the absence (*dotted lines*) or presence (*solid lines*) of different amounts of TFE. *B* and *D* show spectra of Bax$^{\alpha5}$ and Bid$^{\alpha6}$, respectively, in pure aqueous buffer (*dotted lines*) or titrated with increasing amounts of SDS (*solid lines*). In all samples peptides were at a 30 μM concentration, and the aqueous buffer was 10 mM sodium phosphate, pH 7.0. The amounts of added TFE (in percentage) or SDS (in mmol/L) are indicated in the graphs.

precentrifugation ratio of 50, suggesting that virtually all the peptide was associated to the vesicles. With PC LUVs, instead, the estimated *L/P* ratio was ~110, indicating a two-fold lower association. The relative affinity of Bax$^{\alpha5}$ for the two lipid compositions showed the same trend, but was in both cases ~1.5 times lower than in the case of Bid$^{\alpha6}$ (Table 3).

Compared to the situation in aqueous buffer, we observed, for both peptides, a significant decrease of the aggregated portion upon binding to PC/PA LUVs, suggesting that they bind to the membranes in the nonaggregated form. In this nonaggregated portion, an increase in α-helical composition was also evident, at the expense of β-turn and random structures (Fig. 6 and Table 3).

From the 0° and 90° polarized spectra of the inserted peptide, it was possible to calculate the dichroic ratio of the helices and the orientation of their main axis with respect to the perpendicular to the plane of the membrane (Menestrina, 2000). With PC/PA LUVs we obtained an average tilt angle ($\gamma_\perp$) of 46° for Bid$^{\alpha6}$, and 55° and 83° for α_1 and α_2, respectively, of Bax$^{\alpha5}$ (Table 4). When we considered the average orientation of the lipid chains, their tilt angle was found to be 34° in the absence of peptides, and increased to 38° in the presence of Bid$^{\alpha6}$ and to 41° in the presence of Bax$^{\alpha5}$. This finding means that the binding of the peptides increases lipid disorder. The tilt angles of the lipid chains were used to recalculate the relative orientation of the helices with respect to the axis of the lipid chains (Menestrina, 2000), providing an angle (γ_L) of ~34° for Bid$^{\alpha6}$ and ~59° and 90° for α_1 and α_2, respectively, of Bax$^{\alpha5}$ (Table 4).

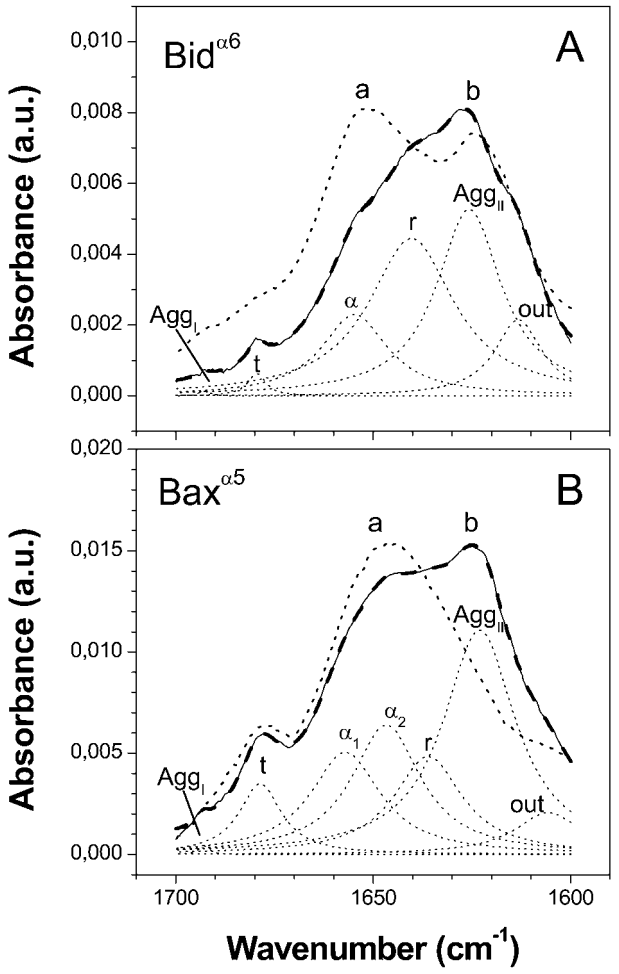

FIGURE 5 Infrared attenuated total reflection spectra of Bid$^{\alpha6}$ and Bax$^{\alpha5}$ in aqueous buffer or TFE solvent. (*A*) Analysis of the amide I′ band of deuterated films of Bid$^{\alpha6}$ samples deposited from TFE (*curve a*) and from a buffer solution (*curve b*). The original spectrum (*solid line* in *b*) was deconvoluted and curve fitted to resolve the component frequencies. The corresponding Lorentzian bands are reported as dotted lines and their sum (*thick dashed line*) was superimposed to the original spectrum. Bands labeled as Agg_I and Agg_{II} derive from aggregated peptide and were excluded from the secondary structure calculation. The other bands are *t* (β-turn), α_1 and α_2 (α-helix), and *r* (random coil). The evaluated percentages of secondary structures are reported in Table 3. (*B*) Same as in *A*, but for the Bax$^{\alpha5}$ peptide.

In the case of the PC LUVs, the lipid chains had already an average tilt of ~42° with respect to the normal of the membrane plane, and this did not change appreciably upon binding of the peptides, which is consistent with the lower binding observed. The orientation of the α-helical structures with respect to the lipid chains was ~50° for Bid$^{\alpha6}$, i.e., less inserted than with PC/PA, and ~0° and 90° for α_1 and α_2, respectively, of Bax$^{\alpha5}$. This suggests that in the case of Bax$^{\alpha5}$ the distorted α-helix, α_2, seems to be oriented parallel to the membrane surface independently of the lipid composition, whereas the regular α-helix, α_1, appears fully immersed in the lipid matrix and its tilt decreases when negatively charged lipids are present.

DISCUSSION

The regulation of release of apoptotic factors from the mitochondria involves alteration of the permeability properties of the outer membrane of this organelle, which is believed to be performed by proteins of the Bcl-2 family. Members of this clan, like Bax and Bid, can form ion channels and permeabilize lipid vesicles to large molecules in a way that is, however, still not well understood at the molecular level. Similar to the pore-forming domain of colicins and other bacterial toxins, there exists in most Bcl-2 proteins a hairpin of two hydrophobic α-helices that are considered to be responsible for membrane insertion and pore formation. We have previously demonstrated that the first fragment of the hairpin of Bax and Bid, namely α-helices 5 and 6, respectively, has the capacity to insert across natural lipid bilayers in the absence of the rest of the protein (García-Sáez et al., 2004). Continuing with such a reductionist approach, the structure and poration activity of the Bax$^{\alpha5}$ and Bid$^{\alpha6}$ protein fragments are reported here.

The structure of Bax$^{\alpha5}$ and Bid$^{\alpha6}$ is investigated in the lipid-mimetic conditions provided by TFE and SDS, as well as in the lipidic environment of PC and PC/PA liposomes. Although both peptides are soluble in water, they show a large proportion of either random-coil or aggregated structures at those conditions. In contrast, the structure is predominantly α-helical in lipid-mimetic and lipidic environments. This is clearly observed in the CD spectra (Fig. 4 and Results), and in a more quantitative way from the FTIR analysis (Table 4). The large amounts of β-type aggregated peptides observed by FTIR, as compared to CD, may be explained by the different sample conditions used for each case. Thus, although samples for CD measurements were of low concentration and completely dissolved, in the case of FTIR measurements, aggregates may have built up while drying the samples during the preparation of the films over the germanium crystals. This water depletion could improve the hydrophobic interactions between peptides and stabilize the helical structure, which may explain the high helical content measured by FTIR for the Bax peptide in buffer.

The negatively charged PC/PA vesicles solubilize a larger amount of aggregated peptide, either Bax$^{\alpha5}$ or Bid$^{\alpha6}$, than the neutral PC vesicles, showing the influence of lipid charge in enhancing the interaction of these positively charged peptides with negatively charged membranes. It appears, however, that the neutral PC LUVs induce a higher amount of α-helix for both peptides (Table 3). On the other hand, the amide I′ frequencies reveal the existence of two types of helices in the case of Bax$^{\alpha5}$, both of them distinguished by their relative orientation in PC and PC/PA LUVs (Table 4). A different pattern is observed for Bid$^{\alpha6}$, where a single type of α-helix aligns tilted with respect to the membrane normal.

TABLE 3 FTIR spectroscopic determination of the secondary structure of Bid$^{\alpha 6}$ and Bax$^{\alpha 5}$ in aqueous buffer, with and without lipids, and in TFE solvent

	Protein	Medium	% Secondary structure*				% βAgg†	L/P‡
			t	*α*	*r*			
		Wavenumber (cm^{-1})	1681 ± 1	1655 ± 2	1642 ± 3			
Bid$^{\alpha 6}$		buffer	2	29	69		39	
		TFE	7	74	18		42	
	+ LUVs	PC	—	72	28		49	110
		PC/PA (1:1)	—	60	40		21	56
			% Secondary structure*					
			t	α_1	α_2	*r*		
		Wavenumber (cm^{-1})	1680 ± 2	1656 ± 1	1646 ± 1	1636 ± 1		
Bax$^{\alpha 5}$		buffer	12	28	34	26	37	
		TFE	13	27	33	27	17	
	+ LUVs	PC	5	38	47	10	34	160
		PC/PA (1:1)	—	32	43	25	9	80

*Percentages refer to the nonaggregated peptide. *t*, β-turn; α, α_1, and α_2, α-helix; *r*, random coil.
†βAgg, total aggregated peptide calculated from the relative areas of the corresponding Lorentzian bands (Agg_I and Agg_{II} in Fig. 5).
‡*L/P*, lipid/peptide molar ratio.

We have also found that both Bax$^{\alpha 5}$ and Bid$^{\alpha 6}$ induce the release of calcein from lipidic vesicles and form ion-conducting channels in planar lipid bilayers at a physiological pH and at concentrations close to those reported for the full-length proteins. However, the two peptides behave differently when we study the effect of the lipid composition in LUVs or the pattern of channel formation in planar bilayers. These facts, together with their distinct pattern of orientation with respect to the membrane plane, suggest that they follow different permeabilization mechanisms.

In the case of Bax$^{\alpha 5}$, the data indicate that this peptide induces the formation of lipidic (or partially lipidic) pores of toroidal-like structure. The induced release of calcein from lipid vesicles is markedly enhanced by the positively curved LPC and barely enhanced by the negatively curved PE. Additionally, when the two types of lipids are simultaneously present, PE appears to exert some attenuation over the enhancing activity of LPC (Table 1). Because of its geometry, a toroidal pore is characterized by positive curvature at the place of monolayer fusion, as well as

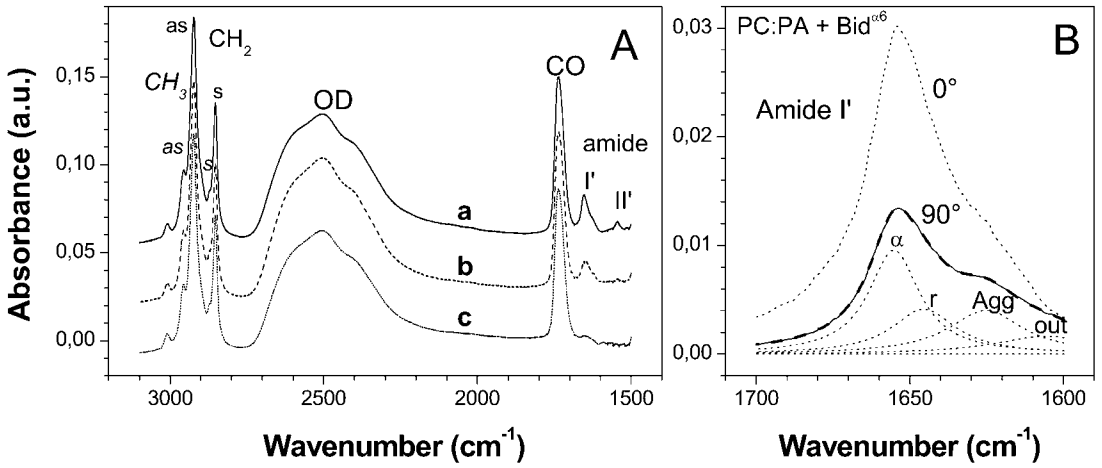

FIGURE 6 ATR-FTIR spectra of Bid$^{\alpha 6}$ and Bax$^{\alpha 5}$ in PC/PA layers and their analysis with polarizer. (*A*) Deuterated films of Bid$^{\alpha 6}$ bound to PC/PA vesicles (***a***, *solid line*), Bax$^{\alpha 5}$ bound to PC/PA vesicles (***b***, *dashed line*) and PC/PA vesicles alone (***c***, *dotted line*). Indicated are the bands corresponding to CH_3 stretching (asymmetric, *as*, and symmetric, *s*, at 2956 cm^{-1} and 2872 cm^{-1}, respectively); CH_2 stretching (asymmetric, *as*, and symmetric, *s*, at 2923 cm^{-1} and 2853 cm^{-1}, respectively); OD stretching of deuterated water; CO stretching of the phospholipid carbonyl groups; amide I′ and II′ bands. (*B*) Spectra were taken with either parallel (*0°*) or perpendicular (*90°*) polarization. The amide I′ region of Bid$^{\alpha 6}$ bound to PC/PA vesicles was reported after subtraction of the lipid contribution. The best curve fit with Lorentzian components (*dotted lines*) was superimposed as a thick dashed line to the 90° polarized trace (*solid line*). The absorption bands in the parallel and perpendicular configuration were used to calculate the orientation of the corresponding structural element as reported in Table 4. Bands are α, α-helix; *r*, random coil; and *Agg*, aggregated peptide.

TABLE 4 Orientation of the helical elements of Bid$^{\alpha 6}$ and Bax$^{\alpha 5}$ bound to PC and PC/PA membranes, and assignment and dichroic ratio of some relevant infrared bands

			PC				PC/PA (1:1)			
Wavenumber (cm^{-1})	Vibration*	Direction (θ)†	Dichroic ratio	Form factor (S)	Angle ($\gamma_\perp$)‡	Angle (γ_L)§	Dichroic ratio	Form factor (S)	Angle ($\gamma_\perp$)‡	Angle (γ_L)¶
Lipid alone										
2920	*as* CH_2 stretching	90°	1.59 ± 0.01	0.31 ± 0.01	43° ± 1°	-	1.36 ± 0.01	0.51 ± 0.01	34° ± 1°	-
2850	*s* CH_2 stretching	90°	1.56 ± 0.01	0.33 ± 0.01	42° ± 1°	-	1.34 ± 0.01	0.53 ± 0.01	34° ± 1°	-
2870	*s* CH_3 stretching	0°	3.20 ± 0.70	0.25 ± 0.13	45° ± 5°	-	4.50 ± 0.90	0.42 ± 0.09	38° ± 4°	-
Bid$^{\alpha 6}$										
2920	*as* CH_2 stretching	90°	1.53 ± 0.01	0.35 ± 0.01	41° ± 1°	-	1.46 ± 0.01	0.42 ± 0.01	38° ± 1°	-
2850	*s* CH_2 stretching	90°	1.49 ± 0.01	0.39 ± 0.01	40° ± 1°	-	1.42 ± 0.01	0.45 ± 0.01	37° ± 1°	-
2870	*s* CH_3 stretching	0°	3.90 ± 0.70	0.36 ± 0.08	40° ± 4°	-	3.80 ± 0.60	0.34 ± 0.11	41° ± 4°	-
1655	Amide I′ α-helix	30°	2.10 ± 0.10	0.04 ± 0.05	53° ± 2°	50° ± 5°	2.58 ± 0.03	0.24 ± 0.01	46° ± 1°	34° ± 2°
Bax$^{\alpha 5}$										
2920	*as* CH_2 stretching	90°	1.51 ± 0.01	0.36 ± 0.01	40° ± 1°	—	1.53 ± 0.01	0.35 ± 0.01	41° ± 1°	—
2850	*s* CH_2 stretching	90°	1.48 ± 0.01	0.40 ± 0.01	39° ± 1°	—	1.50 ± 0.01	0.38 ± 0.01	40° ± 1°	—
2870	*s* CH_3 stretching	0°	3.40 ± 0.80	0.27 ± 0.13	44° ± 4°	—	3.50 ± 0.80	0.29 ± 0.18	43° ± 4°	—
1656	Amide I′ α_1-helix	30°	3.64 ± 0.22	0.52 ± 0.04	34° ± 2°	0° ± 2°	1.92 ± 0.01	−0.04 ± 0.01	55° ± 2°	59° ± 2°
1646	Amide I′ α_2-helix	30°	1.30 ± 0.10	−0.40 ± 0.10	80°± 10°	90° ± 2°	1.22 ± 0.01	−0.46 ± 0.01	83° ± 2°	90° ± 2°

*Vibrations are represented as *s*, symmetric, or *as*, asymmetric.
†Direction of the variation of the dipole moment associated with the vibration with respect to the direction of the main molecular axis (aliphatic chain or α-helix axis).
‡Average angle between the direction of the molecular axis and the perpendicular to the crystal plane (i.e., the membrane plane).
§Average angle between the directions of the α-helix axis and the lipid chain axis.

negative curvature all around the pore rim (Alvarez et al., 2001). However, the negative curvature is large only for very small pores, and decreases as the pore radius increases. In contrast, positive curvature stress will increase with the pore radius, being normally the dominant effect. Thus, although lipids with intrinsic positive curvature should generally favor pore formation, negatively curved lipids are expected to favor small-sized pores but oppose large pores. For example, small amounts of negatively cone-shaped lipids have been shown to favor the small pore formed by sticholysins (~1 nm radius), which is proposed to be of toroidal nature (Alvarez et al., 2001). In contrast, the much larger proteolipidic pores formed by full-length Bax, allowing passage of at least 70 kDa dextrans (~5.9 nm Stocks radius), are inhibited by lipids with intrinsic negative curvature (Basanez et al., 2001; Terrones et al., 2004). In line with these ideas, the increased activity of the Bax$^{\alpha 5}$ peptide in the presence of LPC, as observed here, suggests a reduction of the positive curvature stress of toroidal pores formed by this peptide. Additionally, the weak increase of activity observed for PC/PE LUVs, compared with pure PC LUVs, and the reduction of activity in PC/PE/LPC LUVs, compared with PC/LPC LUVs, indicates that the toroidal pores induced by the Bax$^{\alpha 5}$ peptide are of moderate size.

The characteristics of the ion channel activity observed on planar lipid bilayers adds support to a Bax$^{\alpha 5}$-induced lipidic (or mixed lipidic/peptidic) pore. We note here the formation of a large-conductance pore through a two-stage process, and especially the dependence of the ionic selectivity of this pore on net lipid charge (Table 2). A general mechanism of formation of toroidal lipidic/peptidic pores by amphipathic, positively charged peptides has been recently formulated by H. W. Huang (Huang et al., 2004). According to this model, the formation of pores depends on a fine balance between two opposite forces: a membrane tension, σ, representing a stress on the surface of the membrane, which favors pore formation, and a line tension, γ, related to the curvature stress at the place of monolayer fusion, which opposes the pore. Each of them contributes a term that is a function of the pore radius, R, to the energy of the pore, given by $E_R^0 = 2\pi R\gamma - \pi R^2\sigma$. In the process of pore formation, the peptide can act by affecting both terms in two stages. In the first stage (see column *2* in Fig. 7), the interaction of the peptide at the lipid headgroup region generates a stress (or internal membrane tension) that, past a critical P/L value, ends up inducing the opening of a lipidic pore. Once the pore is open, some peptide molecules change orientation to occupy a membrane-inserted position at (or close to) the rim of the pore (column *3* of Fig. 7). In this new state, the peptide would interact favorably with the pore edge, stabilizing it by diminishing the line-tension term, probably through a reduction of the curvature stress at the place of monolayer fusion (Lee et al., 2004).

Our data fit well in the framework of Huang's mechanism. Thus, measurements of Bax$^{\alpha 5}$ channels in planar lipid membranes show a two-step behavior, suggesting that the peptide attaches initially to the membrane (and presses it in the presence of a positive potential), and, only when it reaches a critical concentration on the surface of the bilayer, inserts to form the large-conductance channel observed. The

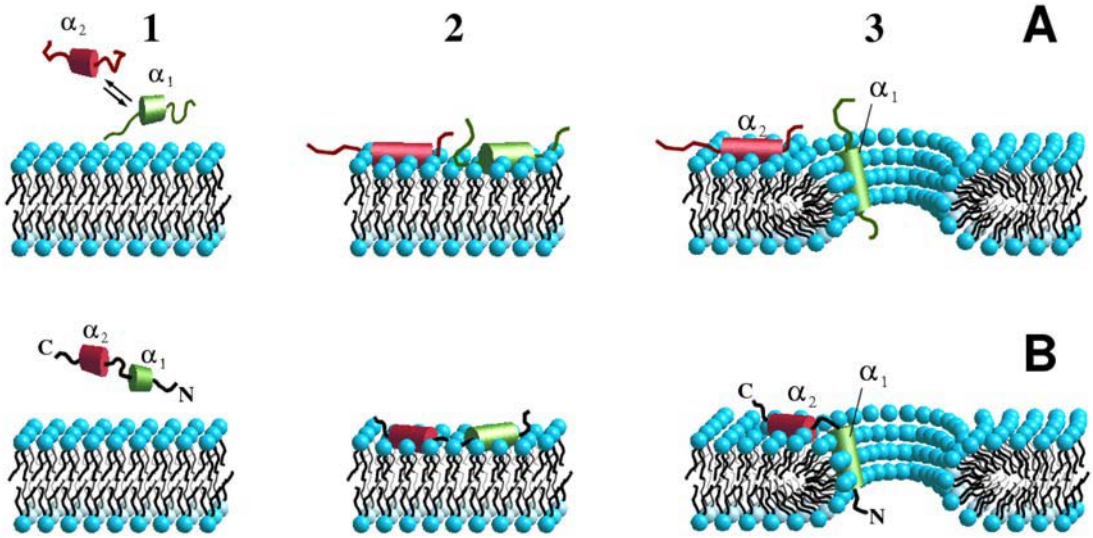

FIGURE 7 Model representing the interaction of Bax$^{\alpha5}$ peptides with lipid membranes and the formation of toroidal pores. (*A*) The two helices, α_1 and α_2, observed by FTIR can be envisioned as an equilibrium between two structural states (column *1*). Both states can interact with membranes (column *2*), creating a tension that induces the opening of a lipidic pore. The state α_1, acquiring a tilted orientation, interacts with the pore edge, which reduces the curvature stress and stabilizes the pore. The state α_2 remains oriented flat at the membrane interface. Alternatively, α_1 and α_2 are two stretches of the same peptide molecule with slightly different α-helical structure (*B*). The pore is formed through the same mechanism as above, but the membrane-inserted state is represented by a kinked peptide, where the part encompassing α_2 remains aligned flat with respect to the membrane plane, whereas the stretch corresponding to α_1 is tilted over the rim of the pore. Helix α_1 can be adscribed to the more hydrophobic, N-terminal half of the peptide (see text).

effect of lipids with intrinsic curvature would be affecting the membrane line tension, being decreased (and the pore favored) by the positively curved LPC (see above).

The existence of two types of α-helix in the case of Bax$^{\alpha5}$, one canonical (α_1) and one distorted (α_2), and their distinct orientation in lipid bilayers, with α_1 tilted (with an angle dependent on lipid composition) and α_2 parallel with respect to the membrane plane (Table 4), can also be discussed in the context of the above mechanism. The two helices can be interpreted as either an equilibrium of two populations of differently structured peptides (Fig. 7 *A*), or two α-helical stretches of different structure within the same peptide molecule (Fig. 7 *B*). Because only helix α_1 is found to be tilted in the lipid samples, the first option would mean that α_1 and α_2 represent membrane-inserted and noninserted states, respectively, of the Bax$^{\alpha5}$ peptide. This, in turn, implies that the two peptide forms interact differently with the membrane, and we would expect that the relative proportion of α_1 with respect to α_2 (α_1/α_2 ratio) changes in the presence of lipid vesicles. However, the α_1/α_2 ratio keeps almost constant (~0.8) regardless of the presence of lipids (Table 3), which makes this first option unlikely. Considering the second option, the percentages of α_1 and α_2 can now be related to the average length of two helical fragments in the 30-residue Bax$^{\alpha5}$ peptide. We can estimate that the regular α-helix, α_1, is ~8 residues long in TFE, whereas the distorted helix, α_2, corresponds to ~10 residues. Both helices increase in a similar proportion as the peptide binds to lipid membranes, up to ~11 and 14 residues for PC LUVs or 10 and 13 residues for PC/PA LUVs, respectively. In the membrane-inserted state, only the stretch encompassing helix α_1 would stick into the bilayer, whereas the stretch α_2 remains flat at the surface. Thus, the species responsible for the stabilization of the pores would be a kinked helical rod (Fig. 7 *B*, column *3*). Since the most hydrophobic part of the peptide is at the N-terminal half, comprising α-helix 5 of parent Bax (residues Gly^{108}–Cys/Ser^{126}), it is likely that the tilted helix α_1 is at this side. Helix α_2 is most likely at the C-terminal half of the assayed peptide, where residues correspond to the turn between helices 5 and 6 of the Bax hairpin. This latter region contains various charged residues and could be organized as an amphipathic structure. The above model may also explain the apparent contradiction between the reduction of the Bax$^{\alpha5}$-induced calcein release in the presence of negatively charged lipids, like PS, PA, and CL (Table 1), and the increased binding of this peptide to negatively charged membranes (PC/PA), determined from the FTIR experiments (Table 3). Thus, a stronger binding to a negatively charged membrane surface may impair pore formation by stabilizing a state with the complete peptide (both helical stretches) aligned flat on the membrane. The smaller average tilt angle determined for helix α1 when bound to PC LUVs, as compared to PC/PA LUVs, is in agreement with this idea. It is also interesting to note that the two types of α-helices are already present in the Bax$^{\alpha5}$ samples in the absence of lipids (although at a lower proportion), suggesting that the structural properties of this peptide are intrinsically prompted for pore formation.

The pattern of poration displayed by Bid$^{\alpha6}$ is clearly different. In this case, only small effects of intrinsic lipid

curvature were observed. However, electrostatic interactions with the membrane seem to determine the action of the peptide. Additionally, Bid$^{\alpha 6}$ forms steplike channels of small size in planar bilayers, and inserts in PC/PA membranes with an average angle of ~34° (~50° for pure PC membranes) with respect to the lipid chains, as deduced from FTIR experiments (Table 4). These observations suggest that Bid$^{\alpha 6}$ may permeabilize the membranes through the formation of barrel-stave channels. However, this appears at first contradictory with recent structural investigations of the interaction of tBid with lipid membranes by electron paramagnetic resonance spectroscopy (Oh et al., 2005) and NMR (Gong et al., 2004), which discard a transmembrane insertion and conclude that binding of the protein takes place, at most, at the interface between the headgroup and acyl-chain regions of the membrane. The electron paramagnetic resonance study shows that α-helix 6 is partially immersed in the membrane, with a number of residues interacting with the hydrophobic region of the bilayer and a small tilt toward the C-terminus. This intimate binding is in fact qualified by the authors as ''insertion'', in contrast to the binding of the more polar α-helices 7 and 8 that lie mainly at the headgroup region (Oh et al., 2005). Thus, it is possible that in the absence of the constraint made by the short connection of helix 6 to the much more polar helix 7, the first one can adopt a deeper insertion, compatible with our observations. It should also be noticed that additional data from the literature report membrane poration activities for tBid that are difficult to explain with an interface binding of the protein (Schendel et al., 1999).

Additionally, we observed that cardiolipin does not seem to exert any special effect other than a small increase in activity that can be attributed to its net negative charge (Table 1). Cardiolipin has been shown to target tBid to the MOM during apoptosis, and a cardiolipin-binding domain, which contains the α-helices 4, 5, and 6, has been defined (Kim et al., 2004). The weak effect of CL on the activity of Bid$^{\alpha 6}$ suggests that the part of the cardiolipin-binding domain responsible for the lipid-protein interaction may lie on α-helices 4 or 5.

Finally, some comment should be added about the implications of our findings for the general understanding of the functional mechanism of the full-length proteins Bax and Bid. As already mentioned, formation of lipidic pores has been reported for Bax and other Bax-like Bcl-2 proteins. These latter pores are accompanied by decreases of bilayer lifetime membrane line tension (Basanez et al., 1999, 2001, 2002; Terrones et al., 2004), strongly suggesting that full-length Bax and the Bax$^{\alpha 5}$ fragment porate membrane bilayers by analogous mechanisms. Similarly, the pores formed by Bid$^{\alpha 6}$ have some parallel with the channel activity of its parent protein (Schendel et al., 1999). This raises the idea that a short peptide encompassing 20–30 residues may carry in its sequence enough structural information to reproduce crucial aspects of the function of a much larger parent protein. It may be particularly so for functions like membrane poration, where the requirements can be provided by only a few residues. From this we can conclude that mechanistic links may exist between simple pore-forming peptides, like antibiotics, and more complex pore-forming proteins, like bacterial toxins and Bcl-2-type apoptotic regulators.

For the two cases studied here, the other putative transmembrane segments of the parent proteins, like helices 1, 6, and 9 in the case of Bax, and helix 7 in the case of Bid, should complete the sketched activity demonstrated by the Bax$^{\alpha 5}$ and Bid$^{\alpha 6}$ fragments. These and other missing parts are essential to give Bax and Bid the complex regulatory faculties that single fragments lack. Nevertheless, the study of the small fragments is important to help in understanding the functioning of the whole, having also the potential to open new ways of exploring possible therapeutic uses.

We thank Enrique Pérez-Payá for helping with the peptide synthesis and critical reading of the manuscript.

This work has been supported by the Generalitat Valenciana (GRUPOS03/202), the Spanish Ministerio de Ciencia y Tecnología (CTQ2004-03444/BQU, BMC2003-01532), the Italian Consiglio Nazionale delle Ricerche, and the Istituto Trentino di Cultura. The Spanish Ministerio de Educación y Cultura is acknowledged for an FPU fellowship to A.J.G.

REFERENCES

Adams, J. M., and S. Cory. 1998. The Bcl-2 protein family: arbiters of cell survival. *Science*. 281:1322–1326.

Alvarez, C., M. Dalla Serra, C. Potrich, I. Bernhart, M. Tejuca, D. Martinez, I. F. Pazos, M. E. Lanio, and G. Menestrina. 2001. Effects of lipid composition on membrane permeabilization by Sticholysin I and II, two cytolysins of the sea anemone *Stichodactyla helianthus*. *Biophys. J.* 80:2761–2774.

Anderluh, G., M. Dalla Serra, G. Viero, G. Guella, P. Macek, and G. Menestrina. 2003. Pore formation by equinatoxin II, an eukaryotic protein toxin, occurs by induction of non-lamellar lipid structures. *J. Biol. Chem.* 278:45216–45223.

Antonsson, B., F. Conti, A. Ciavatta, S. Montessuit, S. Lewis, I. Martinou, L. Bernasconi, A. Bernard, J. J. Mermod, G. Mazzei, K. Maundrell, F. Gambale, R. Sadoul, and J. C. Martinou. 1997. Inhibition of Bax channel-forming activity by Bcl-2. *Science*. 277:370–372.

Axelsen, P. H., B. K. Kaufman, R. N. McElhaney, and R. N. A. H. Lewis. 1995. The infrared dichroism of transmembrane helical polypeptides. *Biophys. J.* 69:2770–2781.

Basanez, G., A. Nechushtan, O. Drozhinin, A. Chanturiya, E. Choe, S. Tutt, K. A. Wood, Y. Hsu, J. Zimmerberg, and R. J. Youle. 1999. Bax, but not Bcl-xL, decreases the lifetime of planar phospholipid bilayer membranes at subnanomolar concentrations. *Proc. Natl. Acad. Sci. USA*. 96:5492–5497.

Basanez, G., J. C. Sharpe, J. Galanis, T. B. Brandt, J. M. Hardwick, and J. Zimmerberg. 2002. Bax-type apoptotic proteins porate pure lipid bilayers through a mechanism sensitive to intrinsic monolayer curvature. *J. Biol. Chem.* 277:49360–49365.

Basanez, G., J. Zhang, B. N. Chau, G. I. Maksaev, V. A. Frolov, T. A. Brandt, J. Burch, J. M. Hardwick, and J. Zimmerberg. 2001. Pro-apoptotic cleavage products of Bcl-x(L) form cytochrome *c*-conducting pores in pure lipid membranes. *J. Biol. Chem.* 276:31083–31091.

Bouillet, P., and A. Strasser. 2002a. Bax and Bak: back-bone of T cell death. *Nat. Immunol.* 3:893–894.

Bouillet, P., and A. Strasser. 2002b. BH3-only proteins—evolutionarily conserved proapoptotic Bcl-2 family members essential for initiating programmed cell death. *J. Cell Sci.* 115:1567–1574.

Chou, J. J., H. Li, G. S. Salvesen, J. Yuan, and G. Wagner. 1999. Solution structure of BID, an intracellular amplifier of apoptotic signaling. *Cell.* 96:615–624.

Dalla Serra, M., and G. Menestrina. 2000. Characterization of molecular properties of pore-forming toxins with planar lipid bilayers. *In* Bacterial Toxins: Methods and Protocols. O. Holst, editor. Humana Press, Totowa, New Jersey. 171–188.

Dalla Serra, M., and G. Menestrina. 2003. Liposomes in study of pore-forming toxins. *Methods Enzymol.* 372:99–124.

Desagher, S., A. Osen-Sand, A. Nichols, R. Eskes, S. Montessuit, S. Lauper, K. Maundrell, B. Antonsson, and J. C. Martinou. 1999. Bid-induced conformational change of Bax is responsible for mitochondrial cytochrome *c* release during apoptosis. *J. Cell Biol.* 144:891–901.

Epand, R. F., J. C. Martinou, M. Fornallaz-Mulhauser, D. W. Hughes, and R. M. Epand. 2002a. The apoptotic protein tBid promotes leakage by altering membrane curvature. *J. Biol. Chem.* 277:32632–32639.

Epand, R. F., J. C. Martinou, S. Montessuit, R. M. Epand, and C. M. Yip. 2002b. Direct evidence for membrane pore formation by the apoptotic protein Bax. *Biochem. Biophys. Res. Commun.* 298:744–749.

Eskes, R., S. Desagher, B. Antonsson, and J. C. Martinou. 2000. Bid induces the oligomerization and insertion of Bax into the outer mitochondrial membrane. *Mol. Cell. Biol.* 20:929–935.

Esposti, M. D., and C. Dive. 2003. Mitochondrial membrane permeabilisation by Bax/Bak. *Biochem. Biophys. Res. Commun.* 304:455–461.

Fisher, L. E., and D. M. Engelman. 2001. High-yield synthesis and purification of an alpha-helical transmembrane domain. *Anal. Biochem.* 293:102–108.

Frey, J., and L. K. Tamm. 1991. Orientation of melittin in phospholipid bilayers. A polarized attenuated total reflection infrared study. *Biophys. J.* 60:922–930.

García-Sáez, A. J., I. Mingarro, E. Perez-Paya, and J. Salgado. 2004. Membrane-insertion fragments of Bcl-x(L), Bax, and Bid. *Biochemistry.* 43:10930–10943.

Gong, X. M., J. Choi, C. M. Franzin, D. Zhai, J. C. Reed, and F. M. Marassi. 2004. Conformation of membrane-associated proapoptotic tBid. *J. Biol. Chem.* 279:28954–28960.

Goormaghtigh, E., V. Raussens, and J. M. Ruysschaert. 1999. Attenuated total reflection infrared spectroscopy of proteins and lipids in biological membranes. *Biochim. Biophys. Acta.* 1422:105–185.

Gordon, L. M., P. W. Mobley, R. Pilpa, M. A. Sherman, and A. J. Waring. 2002. Conformational mapping of the N-terminal peptide of HIV-1 gp41 in membrane environments using C-13-enhanced Fourier transform infrared spectroscopy. *Biochim. Biophys. Acta.* 1559:96–120.

Gross, A., X. M. Yin, K. Wang, M. C. Wei, J. Jockel, C. Milliman, H. Erdjument-Bromage, P. Tempst, and S. J. Korsmeyer. 1999. Caspase cleaved BID targets mitochondria and is required for cytochrome *c* release, while BCL-XL prevents this release but not tumor necrosis factor-R1/Fas death. *J. Biol. Chem.* 274:1156–1163.

Heimlich, G., A. D. McKinnon, K. Bernardo, D. Brdiczka, J. C. Reed, R. Kain, M. Kronke, and J. M. Jurgensmeier. 2004. Bax-induced cytochrome *c* release from mitochondria depends on alpha-helices-5 and -6. *Biochem. J.* 378:247–255.

Hockenbery, D., G. Nunez, C. Milliman, R. D. Schreiber, and S. J. Korsmeyer. 1990. Bcl-2 is an inner mitochondrial membrane protein that blocks programmed cell death. *Nature.* 348:334–336.

Hu, X., Z. Han, J. H. Wyche, and E. A. Hendrickson. 2003. Helix 6 of tBid is necessary but not sufficient for mitochondrial binding activity. *Apoptosis.* 8:277–289.

Huang, H. W., F. Y. Chen, and M. T. Lee. 2004. Molecular mechanism of peptide-induced pores in membranes. *Phys. Rev. Lett.* 92:198304.

Kagawa, Y., and E. Racker. 1971. Partial resolution of the enzymes catalyzing oxidative phosphorilation. XXV. Reconstitution of vesicles catalyzing inorganic phosphorus-32-adenosine triphosphate exchange. *J. Biol. Chem.* 246:5477–5487.

Karbowski, M., Y. J. Lee, B. Gaume, S. Y. Jeong, S. Frank, A. Nechushtan, A. Santel, M. Fuller, C. L. Smith, and R. J. Youle. 2002. Spatial and temporal association of Bax with mitochondrial fission sites, Drp1, and Mfn2 during apoptosis. *J. Cell Biol.* 159:931–938.

Kim, T. H., Y. Zhao, W. X. Ding, J. N. Shin, X. He, Y. W. Seo, J. Chen, H. Rabinowich, A. A. Amoscato, and X. M. Yin. 2004. Bid-cardiolipin interaction at mitochondrial contact site contributes to mitochondrial cristae reorganization and cytochrome *c* release. *Mol. Biol. Cell.* 15: 3061–3072.

Kudla, G., S. Montessuit, R. Eskes, C. Berrier, J. C. Martinou, A. Ghazi, and B. Antonsson. 2000. The destabilization of lipid membranes induced by the C-terminal fragment of caspase 8-cleaved bid is inhibited by the N-terminal fragment. *J. Biol. Chem.* 275:22713–22718.

Kuwana, T., M. R. Mackey, G. Perkins, M. H. Ellisman, M. Latterich, R. Schneiter, D. R. Green, and D. D. Newmeyer. 2002. Bid, bax, and lipids cooperate to form supramolecular openings in the outer mitochondrial membrane. *Cell.* 111:331–342.

Lazebnik, Y. 2001. Why do regulators of apoptosis look like bacterial toxins? *Curr. Biol.* 11:R733–R734.

Lee, M. T., F. Y. Chen, and H. W. Huang. 2004. Energetics of pore formation induced by membrane active peptides. *Biochemistry.* 43:3590–3599.

Lutter, M., M. Fang, X. Luo, M. Nishijima, X. Xie, and X. Wang. 2000. Cardiolipin provides specificity for targeting of tBid to mitochondria. *Nat. Cell Biol.* 2:754–761.

McDonnell, J. M., D. Fushman, C. L. Milliman, S. J. Korsmeyer, and D. Cowburn. 1999. Solution structure of the proapoptotic molecule BID: a structural basis for apoptotic agonists and antagonists. *Cell.* 96: 625–634.

Melnyk, R. A., A. W. Partridge, and C. M. Deber. 2001. Retention of native-like oligomerization states in transmembrane segment peptides: application to the Escherichia coli aspartate receptor. *Biochemistry.* 40:11106–11113.

Menestrina, G. 2000. Use of Fourier-transformed infrared spectroscopy (FTIR) for secondary structure determination of staphylococcal pore-forming toxins. *In* Bacterial Toxins: Methods and Protocols. O. Holst, editor. Humana Press, Totowa, New Jersey. 115–132.

Menestrina, G., V. Cabiaux, and M. Tejuca. 1999. Secondary structure of sea anemone cytolysins in soluble and membrane bound form by infrared spectroscopy. *Biochem. Biophys. Res. Commun.* 254:174–180.

Menikh, A., M. T. Saleh, J. Gariepy, and J. M. Boggs. 1997. Orientation in lipid bilayers of a synthetic peptide representing the C-terminus of the A(1) domain of shiga toxin. A polarized ATR-FTIR study. *Biochemistry.* 36:15865–15872.

Minn, A. J., P. Velez, S. L. Schendel, H. Liang, S. W. Muchmore, S. W. Fesik, M. Fill, and C. B. Thompson. 1997. Bcl-x(L) forms an ion channel in synthetic lipid membranes. *Nature.* 385:353–357.

Muchmore, S. W., M. Sattler, H. Liang, R. P. Meadows, J. E. Harlan, H. S. Yoon, D. Nettesheim, B. S. Chang, C. B. Thompson, S. L. Wong, S. L. Ng, and S. W. Fesik. 1996. X-ray and NMR structure of human Bcl-xL, an inhibitor of programmed cell death. *Nature.* 381:335–341.

Oakes, S. A., J. T. Opferman, T. Pozzan, S. J. Korsmeyer, and L. Scorrano. 2003. Regulation of endoplasmic reticulum Ca2+ dynamics by proapoptotic BCL-2 family members. *Biochem. Pharmacol.* 66:1335–1340.

Oh, K. J., S. Barbuto, N. Meyer, R. S. Kim, R. J. Collier, and S. J. Korsmeyer. 2005. Conformational changes in BID, a pro-apoptotic BCL-2 family member, upon membrane binding. A site-directed spin labeling study. *J. Biol. Chem.* 280:753–767.

Oltvai, Z. N., C. L. Milliman, and S. J. Korsmeyer. 1993. Bcl-2 heterodimerizes in vivo with a conserved homolog, Bax, that accelerates programmed cell death. *Cell.* 74:609–619.

Orzaez, M., J. Salgado, A. Gimenez-Giner, E. Perez-Paya, and I. Mingarro. 2004. Influence of proline residues in transmembrane helix packing. *J. Mol. Biol.* 335:631–640.

Rodionova, N. A., S. A. Tatulian, T. Surrey, F. Jahnig, and L. K. Tamm. 1995. Characterization of two membrane-bound forms of OmpA. *Biochemistry.* 34:1921–1929.

Saito, M., S. J. Korsmeyer, and P. H. Schlesinger. 2000. BAX-dependent transport of cytochrome c reconstituted in pure liposomes. *Nat. Cell Biol.* 2:553–555.

Santos, N. C., and M. A. R. B. Castanho. 1996. Teaching light scattering spectroscopy: the dimension and shape of tobacco mosaic virus. *Biophys. J.* 71:1641–1650.

Schendel, S. L., R. Azimov, K. Pawlowski, A. Godzik, B. L. Kagan, and J. C. Reed. 1999. Ion channel activity of the BH3 only Bcl-2 family member, BID. *J. Biol. Chem.* 274:21932–21936.

Scorrano, L., S. A. Oakes, J. T. Opferman, E. H. Cheng, M. D. Sorcinelli, T. Pozzan, and S. J. Korsmeyer. 2003. BAX and BAK regulation of endoplasmic reticulum Ca2+: a control point for apoptosis. *Science.* 300:135–139.

Sharon, M., Z. Oren, Y. Shai, and J. Anglister. 1999. 2D-NMR and ATR-FTIR study of the structure of a cell-selective diastereomer of melittin and its orientation in phospholipids. *Biochemistry.* 38:15305–15316.

Sreerama, N., and R. W. Woody. 2000. Estimation of protein secondary structure from circular dichroism spectra: comparison of CONTIN, SELCON, and CDSSTR methods with an expanded reference set. *Anal. Biochem.* 287:252–260.

Sreerama, N., and R. W. Woody. 2004. On the analysis of membrane protein circular dichroism spectra. *Protein Sci.* 13:100–112.

Suzuki, M., R. J. Youle, and N. Tjandra. 2000. Structure of Bax: coregulation of dimer formation and intracellular localization. *Cell.* 103:645–654.

Tamm, L. K., and S. A. Tatulian. 1993. Orientation of functional and non-functional PTS permease signal sequence in lipid bilayers. A polarized attenuated total reflection infrared study. *Biochemistry.* 32:7720–7726.

Tamm, L. K., and S. A. Tatulian. 1997. Infrared spectroscopy of proteins and peptides in lipid bilayers. *Q. Rev. Biophys.* 30:365–429.

Terrones, O., B. Antonsson, H. Yamaguchi, H. G. Wang, Y. Liu, R. M. Lee, A. Herrmann, and G. Basanez. 2004. Lipidic pore formation by the concerted action of pro-apoptotic BAX and tBID. *J. Biol. Chem.* 279:30081–30091.

Wolter, K. G., Y. T. Hsu, C. L. Smith, A. Nechushtan, X. G. Xi, and R. J. Youle. 1997. Movement of Bax from the cytosol to mitochondria during apoptosis. *J. Cell Biol.* 139:1281–1292.

Yethon, J. A., R. F. Epand, B. Leber, R. M. Epand, and D. W. Andrews. 2003. Interaction with a membrane surface triggers a reversible conformational change in Bax normally associated with induction of apoptosis. *J. Biol. Chem.* 278:48935–48941.

Zha, J., S. Weiler, K. J. Oh, M. C. Wei, and S. J. Korsmeyer. 2000. Posttranslational N-myristoylation of BID as a molecular switch for targeting mitochondria and apoptosis. *Science.* 290:1761–1765.

Zimmerberg, J., and L. V. Chernomordik. 1999. Membrane fusion. *Adv. Drug Deliv. Rev.* 38:197–205.